Journal of Cleaner Production 501 (2025) 145313

Contents lists available at ScienceDirect

Journal of Cleaner Production

journal homepage: www.elsevier.com/locate/jclepro

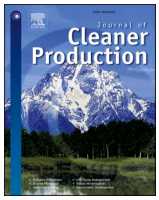

Multifield computational model of chemical recycling of polymer composites: Temperature effects on solvolysis efficiency and energy consumption

Yi Chen [*], Justine Beauson, Asger Bech Abrahamsen, Leon Mishnaevsky Jr. [**]

Department of Wind and Energy Systems, Technical University of Denmark, Roskilde, Denmark

ARTICLE INFO

Handling Editor: Weidong Li

Keywords:
Composite recycling
Solvolysis
Multifield model
Finite element analysis

ABSTRACT

As a promising recycling technology for fiber-reinforced composites (FRCs), solvolysis effectively separates fibers from their polymer matrix. Understanding and predicting the solvolysis process of composites is essential for optimizing recycling technologies and planning end-of-life strategies. This paper proposes a multifield computational model that integrates diffusion, chemical reaction, temperature distribution, and mechanical responses, with a focus on the effect of temperature during solvolysis. The coupled model was numerically implemented using the finite element method and calibrated with experimental data from solvolysis of epoxy resin at various temperatures. The effects of fiber placement and fiber volume fraction on solvolysis was examined using the computational model. Results show that higher fiber volume fractions lead to slower solvolysis, which can be explained by fibers acting as barriers to solvent diffusion into the polymer. The influence of temperature on fiber degradation and energy consumption was also investigated by incorporating an empirical strength degradation equation and a heat conduction model. The strength of recovered fibers decreases from 99 % at 85 °C to 85 % at 300 °C within 40 h, while the energy consumption for solvolysis at 145 °C is 20 % higher than at 85 °C. The findings suggest that optimizing solvolysis conditions, particularly temperature, is crucial for balancing recycling efficiency and maintaining fiber integrity.

1. Introduction

Fiber-reinforced composites (FRCs) are widely used across various industries, including aerospace, automotive, and wind energy (Zhang et al., 2023), (Lou et al., 2023), due to their excellent mechanical properties such as high strength-to-weight ratios and fatigue durability. Driven by rising demand in these sectors, the global FRCs market is projected to grow at a compound annual growth rate (CAGR) of 7.4 % from 2023 to 2031. However, increased demand also results in more composite waste. In Europe alone, 6000 to 8000 commercial planes are expected to retire by 2030 (Khurshid et al., 2020 Stena Recycling, 2023), and over 52000 tons of wind turbine blades will need recycling annually by 2030 (Stena Recycling, 2023). Recycling carbon and glass fiber-reinforced composites has become a crucial concern due to the environmental and economic pressures associated with their disposal (Çelik et al., 2022), (Martínez-García et al., 2022).

The end-of-life management of FRCs poses significant challenges due to their complex structure and the difficulty of separating fibers from the polymer matrix (Mishnaevsky, 2021). Chemical recycling through solvolysis offers a promising solution. Solvolysis involves breaking down the matrix materials using solvents such as water, acetone, alcohols, ammonia, and supercritical fluids. This method enables the recovery of both the matrix and high-quality fibers with retained mechanical properties, allowing their reuse in high-performance applications (Branfoot et al., 2023). Significant research has focused on developing and optimizing solvolysis for recycling glass, carbon, basalt, and aramid fibers from epoxy, unsaturated polyester, and thermoplastic FRCs.

The matrix degradation rate during solvolysis is influenced by temperature, solvent concentration, catalysts, reactor type, pressure, and stirring, with temperature being the most critical factor. Most studies have shown that increasing temperature enhances degradation efficiency, although higher temperatures can sometimes reduce efficiency by forming insoluble char on the fibers (Rani et al., 2022).

Furthermore, solvolysis processes at elevated temperatures can lead

* Corresponding author.
** Corresponding author.
E-mail addresses: yiach@dtu.dk (Y. Chen), lemi@dtu.dk (L. Mishnaevsky).

https://doi.org/10.1016/j.jclepro.2025.145313
Received 7 October 2024; Received in revised form 13 December 2024; Accepted 14 March 2025
Available online 18 March 2025

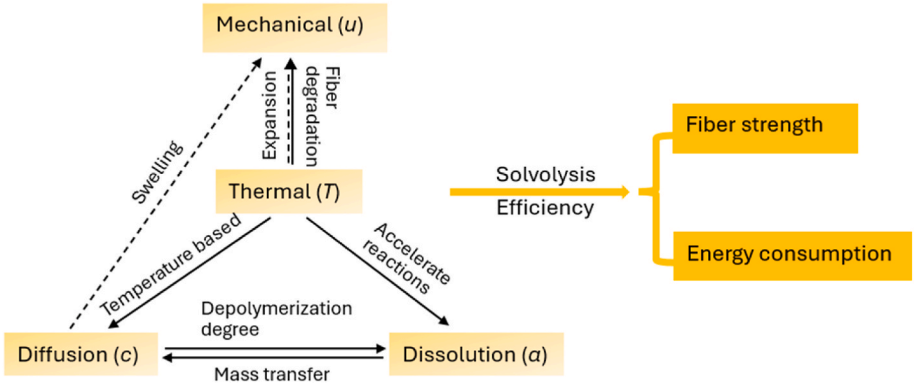

Fig. 1. Schematic of the coupled model and the evaluation of the efficiency of solvolysis process from the perspectives of fiber strength and energy consumption. The dashed arrows indicate components planned for future study.

to surface oxidation of reclaimed fibers, potentially affecting their strength and compatibility with matrix materials (He et al., 2020). Xu et al. proposed a two-step process to recycle carbon fibers from an epoxy composites (Xu et al., 2013). Samples were pretreated with CH_3COOH before undergoing oxidative degradation with a mixture of hydrogen peroxide and dimethylformamide. Results showed that the tensile strength of recovered fibers decreases with increasing temperature, with a 17 % reduction compared to virgin fibers at 135 °C. Li et al. developed a chemical recycling method for carbon fiber/epoxy composites using oxidative degradation with acetone and hydrogen peroxide (H_2O_2) (Li et al., 2012). Below 100 °C, the tensile strength of recovered fibers stayed above 90 % of that of virgin fibers, but it dropped further at 120 °C, indicating greater damage at higher temperatures.

Due to their high thermal sensitivity, glass fibers are more susceptible to degradation at high solvolysis temperatures. Feih et al. investigated the effects of temperature, heating time, and atmosphere on the tensile modulus and strength of thermally treated E-glass fibers (Feih et al., 2011). The tensile strength of the fibers decreased significantly with increasing temperature and prolonged heating time, although the modulus remained unchanged. They also proposed a phenomenological model to predict the residual strength of fibers based on temperature and heating time. Mechanical property degradation with increasing temperature can be exacerbated by the presence of acidic or alkaline solvents/additives (Okajima et al., 2014), (Rijo et al., 2023). This degradation due to the defects induced by chemical reactions involving carbon atoms on fiber surfaces and significant stress heterogeneity (Yan et al., 2016).

Although solvolysis, as a promising disposal method, has attracted increasing attention from researchers for the last decade, it is still on a relatively low readiness level due to low efficiency. Modeling the solvolysis is essential for the design and optimization of recycling strategies, as it enhances the understanding of polymer matrix degradation and provides deep insights into chemical reactions influenced by varying environmental factors. A reliable and comprehensive model also helps reduce the economic and time costs of experimental trials and guides the transition from laboratory-scale to industrial applications by simulating larger systems (Piccinno et al., 2016). Existing models for polymer dissolution vary in complexity and scope. Due to the complexity of polymer dissolution, where polymer molecules cannot be released until the network of entanglements is relaxed or broken (Kong et al., 2021), polymer-solvent mixtures are often considered as systems divided by a liquid-gel interface and a gel-glass interface. These interfaces move because of both solvent penetration and polymer dissolution. Early studies employed empirical models, such as solid-state reaction theory (Khawam and Flanagan, 2006), (Kuang et al., 2018), to provide overall predictions of the dissolution process. Phenomenological models, such as the Stefan boundary model (Chen and Mishnaevsky, 2024) and models incorporating characteristic dissolution times (Peppas et al., 1994), have been used to describe the motion of the liquid-gel and gel-glass boundaries. However, these models do not provide detailed insights into the mechanisms of polymer dissolution. More detailed approaches use decomposition kinetic models that describe chemical reactions between solvents and polymers by tracking changes in functional group or chain segment concentrations (Hamel et al., 2020), (Luo et al., 2023a). While this method enhances understanding of composite recycling mechanisms with various solvents, it requires specific chemical knowledge and coding skills for finite element analysis. Some researchers have explored polymer dissolution mechanisms using field-based approaches, where the multifield system is described in terms of chemical potentials (Larson, 2004) and degrees of freedom for chemical concentration (Wallmersperger et al., 2009). The Arrhenius equation is commonly used to describe the temperature dependence of chemical reactions (Shi et al., 2016), (Chaabani et al., 2017). However, no existing model captures the temperature distribution during the solvolysis process, which may be crucial for large-scale modeling.

In this paper, we develop a numerical model that integrates diffusion, chemical reaction, temperature distribution, and mechanical response for the chemical recycling of composites under varying temperatures. The effects of fiber arrangements, including placement and fiber volume fraction, on polymer dissolution are examined. To gain deeper insights into the influence of temperature on recovered fiber quality and energy consumption, an empirical equation describing fiber strength loss due to heat treatment and a heat transfer system are utilized.

2. Model introduction

This section presents the governing equations for the coupled diffusion-dissolution-thermal-mechanics system, as shown in Fig. 1. The corresponding discrete equations for the coupled model are formulated and solved numerically.

2.1. Governing equations

- Diffusion part

Assuming the Fickian diffusion, the transport of solvent into polymers for an arbitrary control volume V can be described by a partial differential equation (Shen and Springer, 1976):

$$\frac{dc}{dt} - \nabla \cdot D(\nabla c) = 0 \tag{1}$$

where c is the concentration of solvent, ∇ denotes the spatial gradient, and D is the diffusivity of solvent transport into the polymer, which is defined by the Arrhenius law (Yu et al., 2017), (Luo et al., 2023b) as a function of temperature T and dissolved fraction α:

$$D(T,\alpha) = D_0 \, exp\left[-\frac{E_s}{R}\left(\frac{1}{T} - \frac{1}{T_0}\right)\right] exp\left[\beta\alpha^2\right] \tag{2}$$

where E_s is the activation energy for solvent diffusion, R is the gas constant (8.314 J/K), and β is a fitting parameter.

- Dissolution part

To analyze polymer dissolution within solvent, a transient material balance approach was used. Assuming negligible polymer swelling and a volume-conserving process, the local mass balance in an arbitrary domain can be described as

$$\frac{\partial \phi}{\partial t} + \nabla \boldsymbol{J} = \dot{V} \tag{3}$$

where ϕ is the volume fraction of polymer, $\boldsymbol{J}$ is the volume flux, and $\dot{V}$ presents the rate of volumetric change of polymer due to chemical reactions. Ignoring swelling and density changes due to solvent diffusion, ϕ is defined as:

$$\phi = \frac{V_p}{V_0} = \frac{V_0 - V_d}{V_0} = 1 - \frac{V_d}{V_0} = 1 - \alpha \tag{4}$$

where V_p and V_0 are the present and original volume of polymer, respectively. And V_d is the dissolved volume corresponding to the dissolved fraction α.

The volume flux can be described as a function of ϕ in terms of Fick's law:

$$\nabla \boldsymbol{J} = -\nabla \cdot D_p(\nabla \varnothing) = \nabla \cdot D_p(\nabla \alpha) \tag{5}$$

where the diffusivity of polymer, D_p, is expressed by an exponential function of the solvent diffusivity (Vrentas and Vrentas, 1998), such as

$$D_p = De^{-k\phi} = De^{-k(1-\alpha)} \tag{6}$$

where κ is a constant. The production of solvent is assumed to follow a second-order reaction (Khawam and Flanagan, 2006):

$$\dot{V} = g(c) \bullet K(T) \bullet (1-\alpha)^2 = g(c) A_0 e^{-\frac{E_a}{RT}} (1-\alpha)^2 \tag{7}$$

where A_0 is a frequency factor, E_a is the activation energy, and $g(c)$ is a function that determines when the chemical reaction occurs. In this system, the reaction starts when the local solvent concentration exceeds a threshold value, c_{th}:

$$\begin{cases} g(c) = 0, if\ c < c_{th} \\ g(c) = 1, if\ c \geq c_{th} \end{cases} \tag{8}$$

To address convergence issues, the step function is replaced by a continuous curve varying smoothly from 0 to 1 around the interface at c_{th}:

$$g(c) = \frac{1}{2}[1 + tanh(\varphi c - \omega)] \tag{9}$$

where φ and ω are parameters that determine the curve shape and the interface location.

- Heat transfer

Heat distribution in composite materials occurs through heat conduction, which can be described by the heat equation derived from Fourier's law and the conservation of energy (Narasimhan, 1999). The heat conduction equation is given by:

$$\rho c_p \frac{\partial T}{\partial t} - \nabla \cdot k(\nabla T) = 0 \tag{10}$$

where ρ is the material's density, c_p is the specific heat, T is temperature, and k is the thermal conductivity.

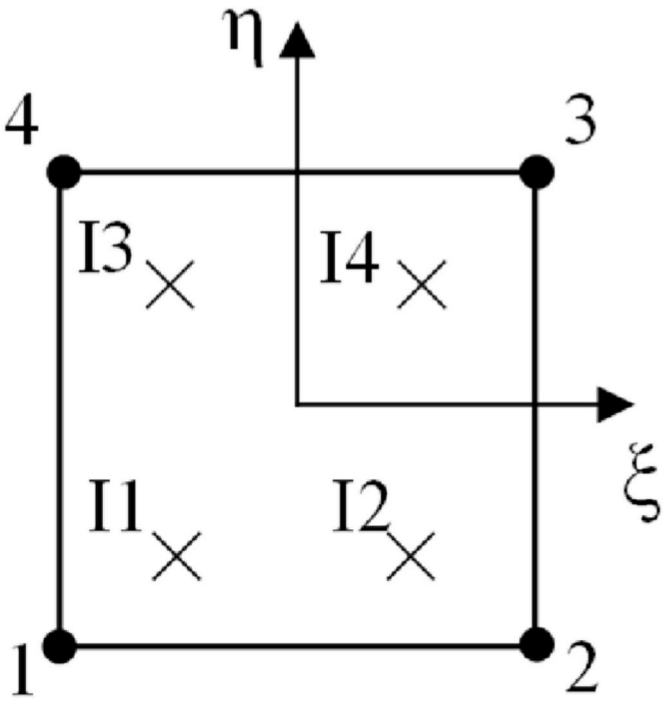

Fig. 2. A two-dimensional element with four nodes and integration points (I1 to I4).

- Mechanical response

The solvent-assisted polymer dissolution process is complex, involving swelling, thermal expansion, and degradation of mechanical properties. In this study, the mechanical response is simplified and described by linear elasticity. It is important to note that the mechanical component of the proposed model, while not directly impacting the study of solvolysis, is essential for a comprehensive modeling of the entire solvolysis system (Fig. 1). The coupled model serves as a framework for the entire solvolysis system and can be further modified in future studies to account for swelling and mechanical degradation.

For an arbitrary domain, the equilibrium equation is obtained as (Cui et al., 2021)

$$\nabla \bullet \boldsymbol{\sigma} = \mathbf{0} \tag{11}$$

with the boundary condition:

$$\boldsymbol{P} = \boldsymbol{\sigma} \bullet \mathbf{n} \tag{12}$$

where $\boldsymbol{\sigma}$ is the Cauchy stress tensor, $\boldsymbol{P}$ is the traction vector, and $\boldsymbol{n}$ is the unit normal vector to the interface. Strain tensor $\boldsymbol{\varepsilon}$ is related to the stress by the elastic stiffness matrix:

$$\boldsymbol{\sigma} = \boldsymbol{D}^e \boldsymbol{\varepsilon} \tag{13}$$

where $\boldsymbol{D}^e$ is the elastic stiffness matrix obtained from Hooke's law.

2.2. Numerical implementation

The coupled mechanical-thermal-diffusion-dissolution model was implemented in the finite element package Abaqus 2022 using a user-defined element (UEL) subroutine (Simulia, 2022). To solve the discretized equations, a two-dimensional user element with four nodes and full integration points was developed, as shown in Fig. 2. During each iteration, the tangent stiffness matrices (AMATRX) and residual vectors (RHS) are required by Abaqus to calculate at the integration points to

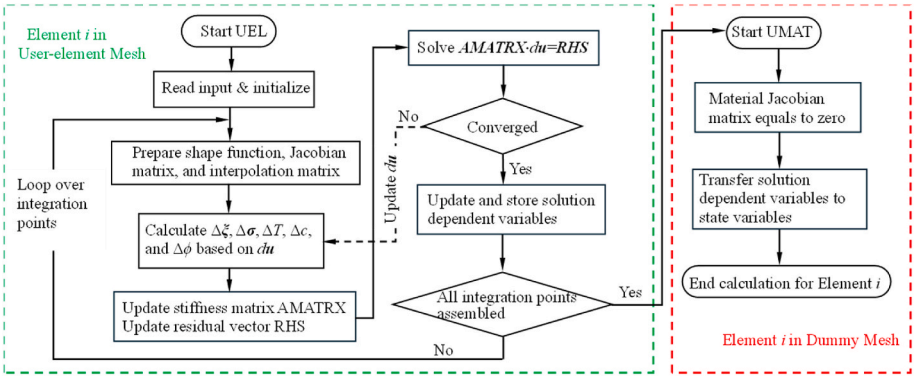

Fig. 3. Flowchart of the calculation process (green frame) and visualization process (red frame) for Element *i* in the finite element system. (For interpretation of the references to colour in this figure legend, the reader is referred to the Web version of this article.)

obtain nodal variables.

To solve the model numerically, the governing equations for the concentration (Eq. (1)), dissolved fraction (Eq. (3)), temperature (Eq. (10)), and displacement (Eq. (11)) are first transformed into their weak forms by multiplying each equation by a test function δ and integrating over the domain, as follows:

$$\int \frac{dc}{dt}\delta_c \, dV + \int D\nabla c\cdot\nabla\delta_c dV = 0 \tag{14}$$

$$\int \frac{\partial\alpha}{\partial t}\delta_\alpha dV + \int D_p\nabla\alpha\cdot\nabla\delta_\alpha dV - \int K(\mathrm{T})f(\alpha)\delta_\alpha \, dV = 0 \tag{15}$$

$$\int \rho c_p\frac{dT}{dt}\delta_T \, dV + \int k\nabla T\cdot\nabla\delta_T dV = 0 \tag{16}$$

$$\int \sigma\delta_\varepsilon \, dV - \int P\cdot\delta_u dS = 0 \tag{17}$$

According to finite element theory, the variables within an element can be obtained from the nodal values using the shape functions:

$$c = \sum_{i=1}^{4}\boldsymbol{N}_i c_i, \alpha = \sum_{i=1}^{4}\boldsymbol{N}_i\alpha_i, T = \sum_{i=1}^{4}\boldsymbol{N}_i T_i, u = \sum_{i=1}^{4}\boldsymbol{N}_i u_i \tag{18}$$

where N_i presents the shape function associated with node *i*. For a four-node fully integrated element, the shape functions are given by

$$\begin{cases} N_1 = \frac{1}{4}(1-\xi)(1-\eta) \\ N_2 = \frac{1}{4}(1+\xi)(1-\eta) \\ N_3 = \frac{1}{4}(1+\xi)(1+\eta) \\ N_4 = \frac{1}{4}(1-\xi)(1+\eta) \end{cases} \tag{19}$$

Similarly, the gradients of the variables are obtained using interpolation matrices $\boldsymbol{B}$, expressed as:

$$\nabla c = \sum_{i=1}^{4}\boldsymbol{B}_i c_i, \nabla\alpha = \sum_{i=1}^{4}\boldsymbol{B}_i\alpha_i, \nabla T = \sum_{i=1}^{4}\boldsymbol{B}_i T_i, \nabla\boldsymbol{\varepsilon} = \sum_{i=1}^{4}\boldsymbol{B}_i^u u_i \tag{20}$$

with $\boldsymbol{B}$ matrices defined as

$$[\boldsymbol{B}_i] = \begin{bmatrix} \frac{\partial N_i}{\partial x} & \frac{\partial N_i}{\partial y} \end{bmatrix}, i = 1,2,3,4 \tag{21}$$

$$[\boldsymbol{B}_i^u] = \begin{bmatrix} \frac{\partial N_i}{\partial x} & 0 \\ 0 & \frac{\partial N_i}{\partial y} \\ 0 & 0 \\ \frac{\partial N_i}{\partial y} & \frac{\partial N_i}{\partial x} \end{bmatrix}, i = 1,2,3,4 \tag{22}$$

Substituting Eqs.(18)–(22) into Eqs.(14)–(17), the residual vectors $\boldsymbol{R}$ are obtained by discretizing the weak forms in time and space:

$$R_{i,c}^{n+1} = \int \frac{c^{n+1}-c^n}{\Delta t}\boldsymbol{N}_i \, dV + \int D\boldsymbol{B}_i^T\left(\nabla c^{n+1}\right)dV \tag{23}$$

$$R_{i,\alpha}^{n+1} = \int \frac{\alpha^{n+1}-\alpha^n}{\Delta t}\boldsymbol{N}_i \, dV + \int D_p\boldsymbol{B}_i^T\left(\nabla\alpha^{n+1}\right)dV - g(c)\int \boldsymbol{K}(T)\boldsymbol{f}(\alpha)\boldsymbol{N}_i dV \tag{24}$$

$$R_{i,\mathrm{T}}^{n+1} = \rho s\int \frac{\mathrm{T}^{n+1}-\mathrm{T}^n}{\Delta t}\boldsymbol{N}_i \, dV + k\int \boldsymbol{B}_i^T\left(\nabla \mathrm{T}^{n+1}\right)dV \tag{25}$$

$$R_{i,\mathrm{u}}^{n+1} = \int \left(\mathbf{B}_\mathbf{i}^\mathbf{u}\right)^{\mathrm{T}}\boldsymbol{\sigma} \, dV - \int \boldsymbol{N}_i^T\boldsymbol{P}dS \tag{26}$$

where the superscripts n and $n+1$ denote the nth and $(n+1)^{\mathrm{th}}$ time steps, and $\Delta t = t^{n+1}\text{-}t^n$ is the time increment. The tangent stiffness matrices are subsequently calculated as:

$$\boldsymbol{K}_{ij,c}^{n+1} = \frac{\partial R_{i,c}^{n+1}}{\partial c_j} = \int \frac{1}{\Delta t}\boldsymbol{N}_i\boldsymbol{N}_j \, dV + \int D\boldsymbol{B}_i^T B_j dV \tag{27}$$

$$\boldsymbol{K}_{ij,\alpha}^{n+1} = \frac{\partial R_{i,\alpha}^{n+1}}{\partial \alpha_j} = \int \frac{1}{\Delta t}\boldsymbol{N}_i\boldsymbol{N}_j \, dV + \int D_p\boldsymbol{B}_i^T B_j dV - g(c)\int K(\mathrm{T})f'(\alpha)\boldsymbol{N}_i\boldsymbol{N}_j dV \tag{28}$$

$$\boldsymbol{K}_{ij,\mathrm{T}}^{n+1} = \frac{\partial R_{i,\mathrm{T}}^{n+1}}{\partial \mathrm{T}_j} = \rho s\int \frac{1}{\Delta t}\boldsymbol{N}_i\boldsymbol{N}_j \, dV + k\int \boldsymbol{B}_i^T B_j dV \tag{29}$$

$$\boldsymbol{K}_{ij,u}^{n+1} = \frac{\partial R_{i,u}^{n+1}}{\partial u_j} = \int \left(\boldsymbol{B}_i^u\right)^T\boldsymbol{D}^e\boldsymbol{B}_j^u dV \tag{30}$$

Therefore, the finite element system can be expressed as

$$\begin{bmatrix} \boldsymbol{K}_u & 0 & 0 & 0 \\ 0 & \boldsymbol{K}_\alpha & 0 & 0 \\ 0 & 0 & \boldsymbol{K}_c & 0 \\ 0 & 0 & 0 & \boldsymbol{K}_T \end{bmatrix}\begin{bmatrix} \boldsymbol{u} \\ \boldsymbol{\alpha} \\ \boldsymbol{c} \\ \boldsymbol{T} \end{bmatrix} = -\begin{bmatrix} \boldsymbol{R}_u \\ \boldsymbol{R}_\alpha \\ \boldsymbol{R}_c \\ \boldsymbol{R}_T \end{bmatrix} \tag{31}$$

Table 1
Parameters in the computational model.

Parameter	Description	Value	Unit
D_0	The reference diffusivity	2×10^{-6}	mm^2/s
β	A constant for diffusivity	0.6	
E_s	A constant related to the dependence of temperature	9×10^6	mJ/mol
κ	A constant for in Eq. 6	50	
E_a	The activation energy	1.3×10^7	mJ/mol
c_0	The constant solvent concentration in the system	1.8×10^{-5}	mol/mm^3
A_0	A frequency factor	10	
φ	A constant in Eq. 9	32	
ω	A constant in Eq. 9	3	
ρ_m	Density of matrix	1.2×10^{-3}	g/mm^3
c_p	Specific heat of matrix	1.1×10^3	mJ/g/K
k_m	Thermal conductivity of matrix	0.17	W/m/K

And it is solved by Newton-Raphson iteration in Abaqus.

2.3. Finite element system

Since Abaqus 2022 does not support the direct visualization of user-defined elements, a 'dummy' mesh was used for visualization of results, overlaid on the user-element mesh. The 'dummy' mesh, constructed with 4-node fully integrated elements (CPE4), shares the same nodes as the user-element mesh and matches the user elements in terms of integration points. During post-processing, numerical results were transferred from the user-defined elements to a user material subroutine (UMAT) defined on the 'dummy' mesh via state variables.

Fig. 3 illustrates the calculation and visualization procedure for an element in the finite element system. Boundary conditions are applied to the dummy mesh. The UEL is first employed to calculate the responses at integration points within the user-defined element. Once the calculation converges, i.e., when the residual vector RHS is below a specified tolerance, the results at the current integration points are updated and stored in the solution-dependent variables. After the results for all integration points within the element are obtained, the UMAT in the corresponding dummy element collects the response data from the user-defined element for visualization. The material Jacobian matrix is set to zero to prevent any influence on the results.

3. Model calibration

The parameters used in the numerical model were determined through solvolysis experiments on epoxy resin PRIME 37 from Gurit (Wattwil, Switzerland). Samples were cured at 65 °C for 7 h and cut into 13 mm × 13 mm × 4 mm dimensions. Solvolysis was performed using a sulfuric acid aqueous solution prepared by dilution with demineralized water. The solvent concentration was 18.1 mol/L, and the solvolysis temperatures were set at 85 °C, 115 °C, and 145 °C. The detailed curing processing and experimental procedure can be found elsewhere (Tortorici et al., 2025).

Using the proposed coupling model, a symmetric model measuring 6.5 mm × 2 mm was created and meshed with 8150 elements in Abaqus (2022). Due to the absence of diffusion tests and to simplify the procedure, the model calibration primarily focused on parameters related to diffusivity and dissolution component. As mentioned previously, the mechanical component serves as an interface for further model modifications, especially to incorporate swelling and mechanical degradation. In this study, it doesn't directly impact the solvolysis results. Therefore, the mechanical properties were assumed to be similar to other epoxy resin and were obtained from reference (Zeng et al., 2017), while the thermal properties were derived from typical values reported in reference (Biercuk et al., 2002). The values for the parameters are listed in Table 1.

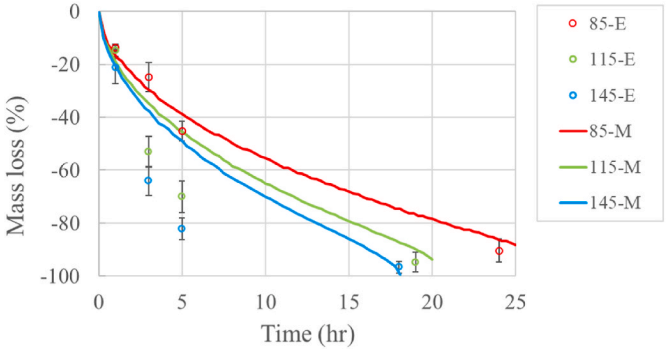

Fig. 4. Comparison of the solvolysis process between experimental data and model predictions (dashed lines) at 85 °C, 115 °C, and 145 °C.

Fig. 4 shows the model's fit to the dissolution process of samples subjected to different temperature levels, specifically under processing conditions of 7 h at 65 °C. At 85 °C, the modeling results align well with the experimental data throughout the dissolution process, demonstrating its capability to accurately capture the behavior at this temperature. However, at 115 °C and 145 °C, the model's predictions start to slightly diverge from the experimental results after 3 h, though they eventually align by the end of the observation period. This discrepancy might be introduced by a more complex relationship between diffusivity and solvolysis temperature, suggesting the need for additional diffusion experiments to accurately define this relationship.

Fig. 5 compares solvent diffusion and temperature distribution within a resin sample after 20 s of solvolysis at 145 °C. The contour of normalized concentration shows blue regions, which indicate areas with no solvent penetration, suggesting that the solvent has barely penetrated the resin. In contrast to solvent diffusion, the temperature distribution exhibits significant variation within the same time period, demonstrating that heat has been effectively transferred throughout the sample. This comparison suggests that, during the solvolysis of a small-scale sample, the temperature can be considered uniform as it reaches equilibrium much faster than the solvent diffuses. A key factor in enhancing the efficiency of chemical recycling methods is the transition from laboratory-scale to industrial applications. In such large-scale systems, where achieving a uniform temperature field requires significantly longer times, temperature gradients become an important role, as they affect both the local diffusivity of solvent molecules and the chemical reaction rates (Wiegand, 2004). Further studies are needed to investigate the influence of temperature gradients on large-scale solvolysis processes.

4. Effect of composite characteristics on solvolysis duration

4.1. Effect of fiber placement on solvolysis duration

Using the calibrated parameters, the combined model was employed to study the solvolysis of composites with randomly distributed fibers. The composite models were designed with dimensions of 0.08 mm in both length and width. Fibers, with a volume fraction of 40 %, were distributed using a random removal algorithm (Park et al., 2018), as shown in Fig. 6. The fiber placement algorithm first generates a master representative volume element (RVE) filled with fibers, and then randomly removes fibers (indicated by yellow dashed circles in Fig. 6) until the desired volume fraction is achieved.

To investigate the effect of fiber placement on solvolysis, four models with randomly distributed fibers were generated, as shown in Fig. 7. Governing the small scale of the model and our focus on the depolymerization mechanism, it was assumed that the solvent was transported from the top surface. The simulated dissolution process of the matrix is depicted in Fig. 8, showing an average mass loss curve over time with

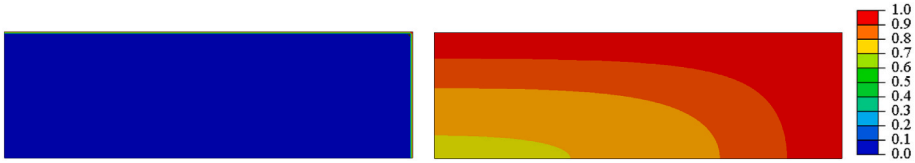

Fig. 5. Comparison of normalized solvent concentration (left) and normalized temperature (right) within a resin sample at 20 s during the solvolysis at 145 °C.

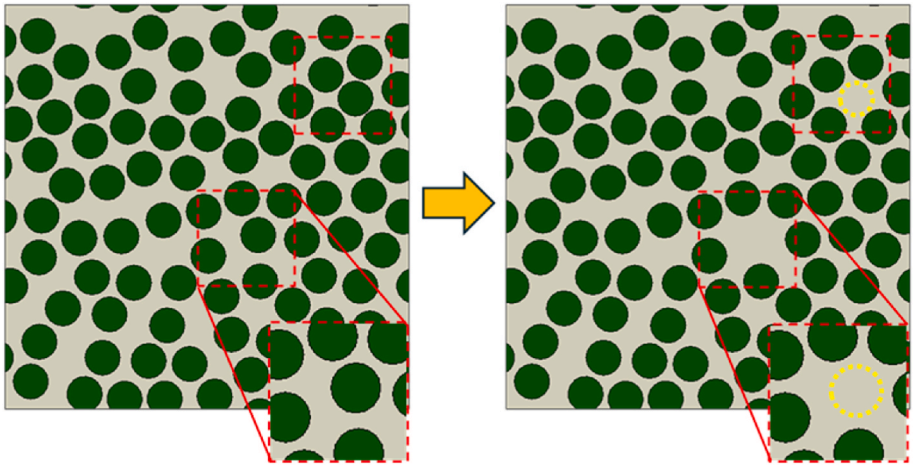

Fig. 6. RVE configuration of the finite element model with fibers randomly distributed via the random removal algorithm.

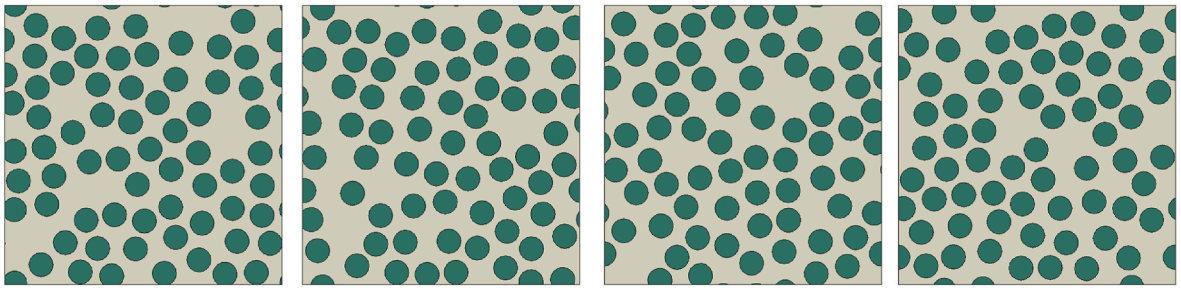

Fig. 7. Random distributions of fibers with a volume fraction of 40 %.

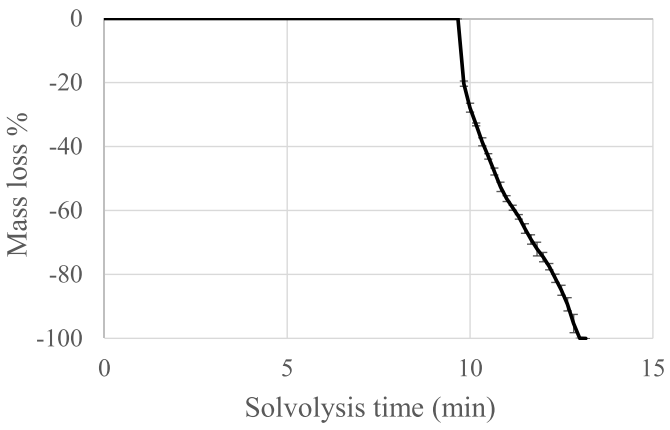

Fig. 8. Comparison of the solvolysis process with varying fiber placements.

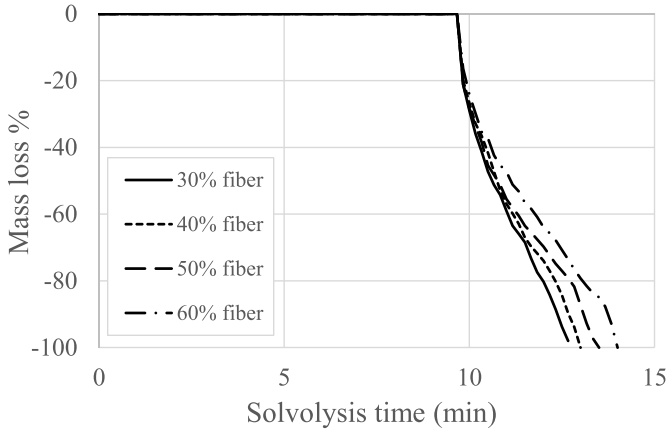

Fig. 9. Predicted solvolysis of the RVE model with fiber volume fractions of 30 %, 40 %, 50 %, and 60 % over time.

standard deviation. The results indicate that fiber displacement has little impact on the dissolution process, with similar outcomes observed across different fiber placements. During the first 9 min, no significant mass loss is detected, suggesting that the solvent requires time to penetrate and initiate the breakdown of the matrix. Once solvolysis begins, the mass loss increases sharply, with the process completing within 13 min.

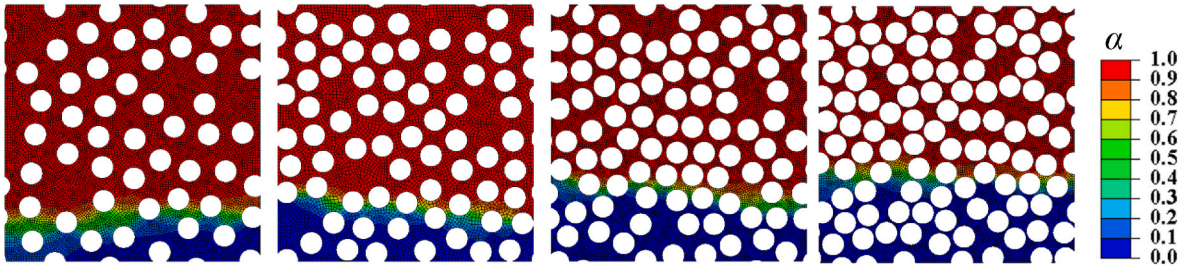

Fig. 10. Simulated depolymerization of the RVE model with fiber volume fractions of 30 %, 40 %, 50 % and 60 % at 4 min. The contour refers to the dissolved fraction.

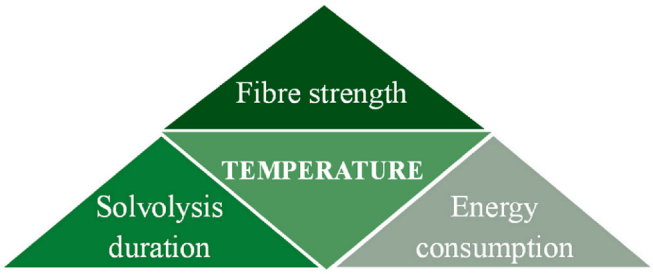

Fig. 11. Temperature affecting fiber strength, solvolysis duration, and energy consumption during solvolysis.

4.2. Effect of fiber volume fraction on solvolysis duration

To study the effect of fiber volume fraction on the solvolysis process, a two-dimensional model measuring 0.08 mm × 0.08 mm with fiber volume fractions of 30 %, 40 %, 50 %, and 60 % was considered. Similar to the model related to fiber placement, the solvent and heat transfer were assumed to occur from the top surface. Fig. 9 shows the predicted solvolysis process of a RVE model at varying fiber volume fractions (30 %, 40 %, 50 %, and 60 %) over solvolysis time, while Fig. 10 shows the simulated appearance of the RVE models at the fourth minute of solvolysis process.

For all fiber fractions, dissolution initiates around the ninth minute. Lower fiber fractions exhibit a faster rate of mass loss compared to higher fractions; for instance, the 30 % fiber fraction reaches total dissolution at 13 min, while the 60 % fiber fraction reaches total dissolution at 14 min. This trend aligns with experimental observations elsewhere (Luo et al., 2023b), (Branfoot et al., 2023), and may be due to higher fiber content resisting solvent access into the polymer matrix, leading to a slower rate of mass loss (Branfoot et al., 2023). However, several studies have shown that longitudinal diffusion is faster than transverse diffusion due to a more tortuous path in the transverse direction (Barjasteh and Nutt, 2012), a fiber-matrix interphase with less dense crosslinking and localized plasticization (Joliff et al., 2014), and weak or debonded interfaces between fibers and the matrix (Gagani et al., 2018). In some cases, longitudinal diffusion rates can be up to 20 times greater than transverse diffusion (Joliff et al., 2014), significantly influencing the overall dissolution rate within the samples. This may result in an opposite observation, where higher fiber content facilitates faster depolymerizing.

Due to the complexity of a multifield model and the high computational cost, the proposed model is two-dimensional and does not consider diffusion along the fiber length (longitudinal diffusion). The simulated results only show that fibers act as barriers to solvent diffusion in the transverse direction. Expanding the model to three dimensions is necessary for a comprehensive study of the solvolysis.

Table 2
Parameters of fiber strength model (Feih et al., 2011).

Parameter	Value	Unit
$\sigma_f(0)$	562	MPa
$T_{50\ \%}$	403	°C
p_f	6.6×10^{-3}	$°C^{-1}$
K_1	8.6×10^{-6}	s^{-1}
K_2	1.2×10^{-3}	$°C^{-1}$

5. Effect of temperature on recovered fibers and energy consumption

Temperature plays an essential role in solvolysis as shown in Fig. 11. As demonstrated in the previous sections, higher temperatures lead to shorter solvolysis duration. Temperature can also be adjusted to either obtain clean, high-strength recovered fibers or to minimize the energy consumption of the solvolysis process. The following sections discuss the potential of adjusting temperature to optimize the process for recovered fiber strength and energy consumption.

5.1. Effect of temperature on fiber strength

Based on the proposed model, we evaluated the efficiency of solvolysis from the perspectives of fiber degradation and energy consumption, as shown in Fig. 1. A phenomenological model (Feih et al., 2011) that relates residual fiber strength to temperature and solvolysis time is employed to predict the strength of recovered fibers and compare the efficiency of solvolysis conditions. The fiber strength, σ_f, is determined by a hyperbolic tangent function of temperature and time, expressed as:

$$\sigma_f(t,T) = \sigma_{f(0)} - \sigma_{\text{loss}}(T) tan\, h\left[k_f(T)t\right] \tag{32}$$

ehere $\sigma_f(0)$ is the original fiber strength, σ_{loss} describes the strength loss, and k_f(T) is the rate of strength loss. The strength loss is obtained by

$$\sigma_{\text{loss}}(T) = \left(\frac{\sigma_{f(0)} - \sigma_{f(a)}}{2}\right)\left(1 + tan\, h\left[p_f(T - T_{50\ \%})\right]\right) \tag{33}$$

where p_f is a constant, $\sigma_{f(a)}$ is the remaining strength of the glass fiber following heat treatment close to the glass transition temperature of E-glass, and $T_{50\ \%}$ is the temperature at which the fiber loses 50 % of the original strength for long exposure time. The rate of strength loss is given by

$$k_f(T) = k_1 e^{k_2 T} \tag{34}$$

where k_1 and k_2 are constants.

Using the parameters from the reference paper (Feih et al., 2011), as listed in Table 2, a composite model with a fiber volume fraction of 28 % was used to study fiber degradation during solvolysis at varying temperatures. The composite sample was assumed to measure 10 mm × 10 mm × 4 mm and contain 14 layers of unidirectional fibers. To save

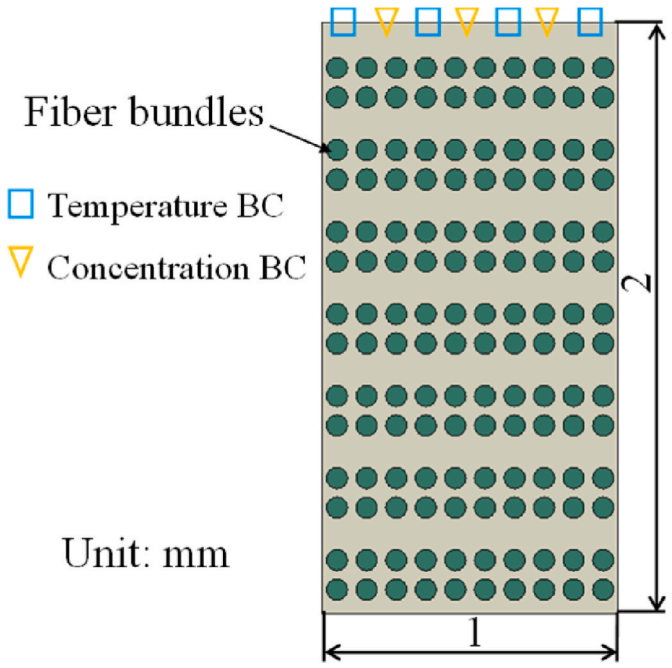

Fig. 12. Schematic of the composites dissolution models with fiber bundles.

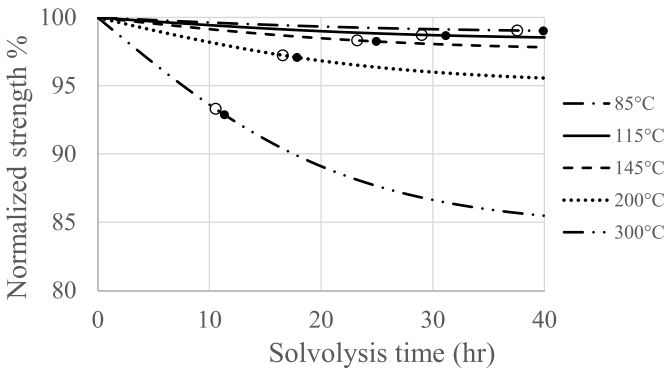

Fig. 13. Strength loss during solvolysis at 85 °C, 115 °C, 145 °C, 200 °C, and 300 °C. Hollow and solid dots present the strength loss when the matrix is 90 % dissolved and fully dissolved, respectively. The parameters of strength loss model are from (Feih et al., 2011).

computational cost, the model was reduced to 1 mm in width and 2 mm in thickness with 7 layers of fibers due to symmetry, as shown in Fig. 12. Simulating the actual number of fibers requires significant computational resources; therefore, the fiber structures were represented as an array of fiber bundles, with each bundle's diameter being fourteen times that of a single fiber (72 μm compared to 5 μm). Each fiber layer was taken to be 0.172 mm thick. Since thermal transfer is significantly faster than solvent diffusion on a small scale, fiber bundles were modeled as inert. Solvent diffusion and temperature distribution were assumed to initiate from the top surface.

Fig. 13 shows the strength loss of fibers over solvolysis time at various temperatures. The results clearly indicate that temperature has a dominant effect on strength loss compared to the duration of exposure, with higher temperatures causing a faster reduction in fiber strength. At 300 °C, the strength drops rapidly to around 85 % within 40 h, while at 85 °C, the strength only decreases to 99 %. This suggests that in applications where maintaining fiber strength is critical, controlling solvolysis temperature is key to optimizing performance and longevity.

Fig. 13 also illustrates the relationship between temperature increase and fiber strength loss when the matrix is 90 % dissolved (hollow dots) and fully dissolved (black dots). As temperature increases, the difference in strength loss between these two dissolution stages becomes more pronounced. For example, at 300 °C, the normalized strength of the 90 % dissolved sample decreases from 93.3 % to 92.8 % for fully dissolved sample within 30 min. The overall strength loss is comparable to the experimental findings, where the recovered glass fibers from solvolysis at 300 °C have a tensile strength of 80–90 % of virgin fibers (Sokoli et al., 2016). However, this model of fiber degradation doesn't consider the effects of acid solvent, and fiber surface corrosion induced by acidic or alkaline environments has been observed (Torkaman et al., 2023), (Bai et al., 2010), implying a potentially higher strength loss. This suggests that in scenarios where the cleanliness of recovered fibers is not a priority, a shorter solvolysis time could be preferred. This would allow for the recovery of higher-quality fibers with more of their strength maintained.

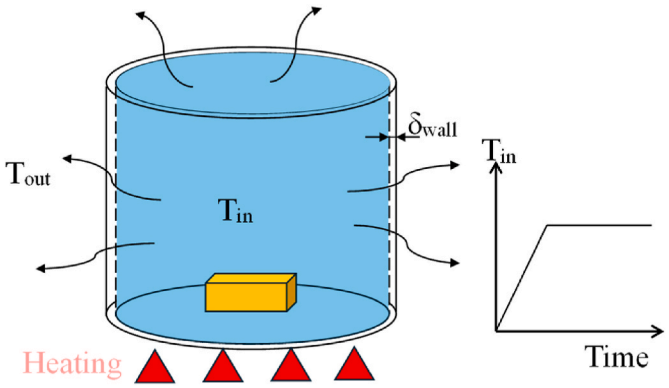

Fig. 14. Sketch of heat transfer during solvolysis.

5.2. Effect of temperature on energy consumption

Based on the results from the previous section, the effect of temperature on energy consumption during solvolysis was studied. Assuming a cylindrical container holding the solvent and composite samples (Fig. 14), an electric heater placed under the container heats the system to the solvolysis temperature and maintains it. Therefore, the energy consumption can be divided into two phases: the heating phase and the temperature maintenance phase. Assuming the efficiency of electricity transfer to heat is 100 %, the energy consumption for solvolysis can be represented by the amount of heat transferred within the system of the heater and container.

Since the sample volume is typically much smaller than the solvent volume, heat transfer considerations focus primarily on the solvent. For the heating phase, the amount of heat gained by the solvent is calculated using the heat transfer formula:

$$Q_H = mc\Delta T \tag{35}$$

where Q_H is the energy gained during the heating phase, m is the mass of solvent, c is the specific heat, and ΔT is the temperature change.

Once the desired temperature is reached, energy continues to be supplied to maintain the temperature, compensating for the heat loss from the container to the surroundings. The corresponding energy input is obtained by a heat conduction model:

$$\dot{Q}_M = kA\frac{T_{in} - T_{out}}{\delta_{wall}} = kA\frac{\Delta T}{\delta_{wall}} \tag{36}$$

where Q_M is the heat loss during the maintenance phase, k is the thermal conductivity of the container material (glass in this study), A is the container area, and δ_{wall} is the container wall thickness.

Therefore, the total electrical energy, E_e, over a time period t can be described as

Table 3
Parameters of heat transfer resulting in electric energy consumption.

Parameter	85 °C	115 °C	145 °C	Unit
A	267			cm^2
δ_{wall}	0.2			cm
T_{out}	20			°C
m	815	804	793	g
c	1.51	1.56	1.61	J/(°C·g)
κ	0.008			W/(°C·cm)
t	39.9	31.1	24.9	h
Ee	27.7	31.6	33.3	kwh

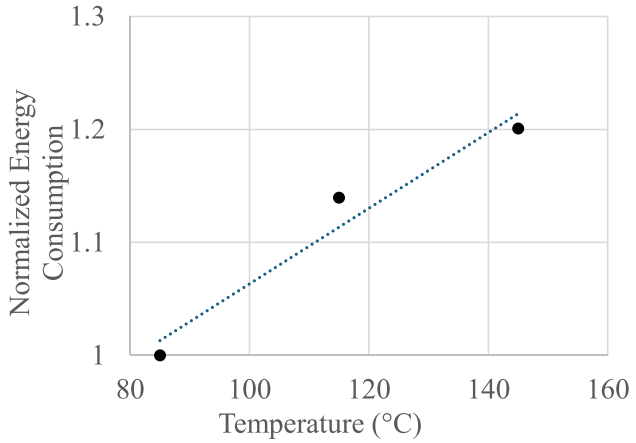

Fig. 15. Comparison of energy consumption of solvolysis at varying temperatures.

$$E_e = Q_H + Q_M = \left(\kappa A \frac{t}{\delta_{wall}} + mc\right)\Delta T \tag{37}$$

The thermal properties and density of the solvent (sulfuric acid aqueous solution with the concentration of 18 mol/L) are temperature-dependent and were obtained from the reference (Bump and Sibbitt, 1955), as listed in Table 3. The container was assumed to have a diameter of 10 cm, a height of 6 cm, and a wall thickness of 0.2 cm. From Fig. 13, the time required for complete matrix dissolution at different temperatures was determined and is also shown in Table 3.

Fig. 15 shows the comparison of energy consumption for solvolysis at different temperatures. It can be observed that energy consumption increases with increasing temperatures. Compared to the linear trend line, which serves as a benchmark, energy consumption increases at a decreasing rate. Specifically, the energy consumed at 115 °C and 145 °C is 14 % and 20 % higher, respectively, than at 85 °C. This trend occurs because energy consumption is determined by both temperature and solvolysis duration, as described by Equation (37). While higher temperatures increase energy consumption, they also reduce the time required for complete matrix dissolution, partially mitigating the total energy demand.

6. Conclusions

This study proposed a computational model integrating diffusion, chemical reaction, temperature distribution and mechanical response to provide a framework for simulating the evolution of composite materials during solvolysis under varying temperature conditions. The model was numerically implemented using the finite element method and calibrated with a series of solvolysis experiments on epoxy resin PRIME 37 at different temperatures. The model was employed to investigate the effect of fiber arrangements on polymer dissolution, demonstrating that fibers act as barriers, resisting solvent getting into polymers and thus slowing the dissolution rate.

The efficiency of solvolysis under different temperature conditions was examined in terms of fiber degradation and energy consumption primarily considering heat transfer. The findings indicate that while higher temperatures accelerate solvolysis, they also reduce the mechanical strength of recovered fibers, highlighting the need to optimize recycling conditions. This study emphasizes the importance of temperature control in maintaining fiber integrity and enhancing recycling efficiency. The modeling effort lays the foundation for multifield modeling of solvolysis of composites and will be extended to further studies to include swelling and thermo-mechanical responses of polymers.

CRediT authorship contribution statement

Yi Chen: Writing – review & editing, Writing – original draft, Visualization, Validation, Methodology, Investigation, Data curation. **Justine Beauson:** Project administration, Funding acquisition, Conceptualization. **Asger Bech Abrahamsen:** Formal analysis, Data curation. **Leon Mishnaevsky:** Supervision, Project administration, Methodology, Investigation, Funding acquisition.

Declaration of competing interest

The authors declare that they have no known competing financial interests or personal relationships that could have appeared to influence the work reported in this paper.

Acknowledgement

The authors acknowledge the financial support of the Innovation Foundation of Denmark in the framework of project “WiseWind: New generation of sustainable wind turbine blades” (wisewind.dtu.dk/), No.2079-00004B. L.M. is grateful to the support of the European Commission via Horizon project “Blades2Build: Recycle, repurpose and reuse end-of-life wind blades composites: A coupled pre- and co-processing demonstration plant”, grant agreement 101096437, and of the Ministry of Foreign Affairs of Denmark via Danida grant 19-M02-DTU “Maintenance and repair strategy for wind energy development” (maintainergy.dk).

Data availability

Data will be made available on request.

References

Bai, Y., Wang, Z., Feng, L., 2010. Chemical recycling of carbon fibers reinforced epoxy resin composites in oxygen in supercritical water. Mater. Des. 31, 999–1002.
Barjasteh, E., Nutt, S.R., 2012. Moisture absorption of unidirectional hybrid composites. Compos. Appl. Sci. Manuf. 43 (1), 158–164.
Biercuk, M.J., Llaguno, M.C., Radosavljevic, M., Hyun, J.K., Johnson, A.T., Fischer, J.E., 2002. Carbon nanotube composites for thermal management. Appl. Phys. Lett. 80 (15), 2767–2769.
Branfoot, C., Folkvord, H., Keith, M., Leeke, G.A., 2023. Recovery of chemical recyclates from fibre-reinforced composites: a review of progress. Polym. Degrad. Stabil. 215 (March).
Bump, T.R., Sibbitt, W.L., 1955. Heat transfer design data–aqueous solutions of nitric acid and of sulfuric acid. Ind. Eng. Chem. 47 (8), 1665–1670.
Çelik, A.İ., et al., 2022. Mechanical behavior of crushed waste glass as replacement of aggregates. Materials 15 (22), 8093.
Chaabani, C., Weiss-Hortala, E., Soudais, Y., 2017. Impact of solvolysis process on both depolymerization kinetics of nylon 6 and recycling carbon fibers from waste composite. Waste and Biomass Valorization 8 (8), 2853–2865.
Chen, Y., Mishnaevsky Jr., L., 2024. Modeling the solvolysis of composite materials of wind turbine blades. Adv. Eng. Mater. 26 (16), 2302150.
Cui, C., Ma, R., Martínez-Pañeda, E., 2021. A phase field formulation for dissolution-driven stress corrosion cracking. J. Mech. Phys. Solid. 147, 104254.
Feih, S., Boiocchi, E., Mathys, G., Mathys, Z., Gibson, A.G., Mouritz, A.P., 2011. Mechanical Properties of Thermally-Treated and Recycled Glass Fibres, *Composite Part B*, vol. 42, pp. 350–358.

Gagani, A., Krauklis, A., Echtermeyer, A.T., 2018. Anisotropic fluid diffusion in carbon fiber reinforced composite rods: experimental, analytical and numerical study. Mar. Struct. 59, 47–59.
Hamel, C.M., Kuang, X., Qi, H.J., 2020. Modeling the dissolution of thermosetting polymers and composites via solvent assisted exchange reactions. Compos. B Eng. 200 (August), 108363.
He, D., et al., 2020. The effect of sizing and surface oxidation on the surface properties and tensile behaviour of recycled carbon fibre: an end-of-life perspective. Compos. Appl. Sci. Manuf. 138, 106072.
Joliff, Y., Rekik, W., Bélec, L., Chailan, J.-F., 2014. Study of the moisture/stress effects on glass fibre/epoxy composite and the impact of the interphase area. Compos. Struct. 108, 876–885.
Khawam, A., Flanagan, D.R., 2006. Solid-state kinetic models: basics and mathematical fundamentals. J. Phys. Chem. B 110 (35), 17315–17328.
Khurshid, M.F., Hengstermann, M., Hasan, M.M.B., Abdkader, A., Cherif, C., 2020. Recent developments in the processing of waste carbon fibre for thermoplastic composites–a review. J. Compos. Mater. 54 (14), 1925–1944.
Kong, D., et al., 2021. Control of polymer properties by entanglement: a review. Macromol. Mater. Eng. 306 (12), 2100536.
Kuang, X., Shi, Q., Zhou, Y., Zhao, Z., Wang, T., Qi, H.J., 2018. Dissolution of epoxy thermosets: via mild alcoholysis: the mechanism and kinetics study. RSC Adv. 8 (3), 1493–1502.
Larson, R.S., 2004. Model for reaction-assisted polymer dissolution in LIGA. J. Appl. Polym. Sci. 97 (1), 25–37.
Li, J., Xu, P.-L., Zhu, Y.-K., Ding, J.-P., Xue, L.-X., Wang, Y.-Z., 2012. A promising strategy for chemical recycling of carbon fiber/thermoset composites: self-accelerating decomposition in a mild oxidative system. Green Chem. 14 (12), 3260–3263.
Lou, Z., et al., 2023. Modification and application of bamboo-based materials: a review—Part II: application of bamboo-based materials. Forests 14 (11), 2266.
Luo, C., Chung, C., Yu, K., 2023a. A diffusion-reaction computational study to reveal the depolymerization mechanisms of epoxy composites for recycling. Mater. Today Sustain. 23, 2–4.
Luo, C., Chung, C., Yu, K., 2023b. A diffusion-reaction computational study to reveal the depolymerization mechanisms of epoxy composites for recycling. Mater. Today Sustain. 23, 100452.
Martínez-García, R., et al., 2022. The present state of the use of waste wood ash as an eco-efficient construction material: a review. Materials 15 (15), 5349.
Mishnaevsky, L., 2021. Sustainable end-of-life management of wind turbine blades: Overview of current and coming solutions. Materials 14 (5), 1124.
Narasimhan, T.N., 1999. Fourier's heat conduction equation: history, influence, and connections. Rev. Geophys. 37 (1), 151–172.
Okajima, I., Hiramatsu, M., Shimamura, Y., Awaya, T., Sako, T., 2014. Chemical recycling of carbon fiber reinforced plastic using supercritical methanol. J. Supercrit. Fluids 91, 68–76.
Park, S.M., Lim, J.H., Seong, M.R., Sohn, D., 2018. Efficient generator of random fiber distribution with diverse volume fractions by random fiber removal. Compos. B Eng. 167, 302–316, 2019.
Peppas, N.A., Wu, J.C., von Meerwall, E.D., 1994. Mathematic modeling and experimental characterization of polymer dissolution. Macromolecules 27, 5626–5638.
Piccinno, F., Hischier, R., Seeger, S., Som, C., 2016. From laboratory to industrial scale: a scale-up framework for chemical processes in life cycle assessment studies. J. Clean. Prod. 135, 1085–1097.
Rani, M., Choudhary, P., Krishnan, V., Zafar, S., 2022. Development of sustainable microwave-based approach to recover glass fibers for wind turbine blades composite waste. Resour. Conserv. Recycl. 179, 106107.
Rijo, B., Dias, A.P.S., Carvalho, J.P.S., 2023. Recovery of carbon fibers from aviation epoxy composites by acid solvolysis. Sustain. Mater. Technol. 35, e00545.
Shen, C.H., Springer, G.S., 1976. Moisture absorption and desorption of composite materials. J. Compos. Mater. 10 (1), 2–20.
Shi, Y., et al., 2016. Solvolysis kinetics of three components of biomass using polyhydric alcohols as solvents. Bioresour. Technol. 221, 102–110.
Simulia, 2022. Abaqus User Subroutines Reference Guide. Dassault Système.
Sokoli, H.U., Simonsen, M.E., Nielsen, R.P., Arturi, K.R., Søgaard, E.G., 2016. Conversion of the matrix in glass fiber reinforced composites into a high heating value oil and other valuable feedstocks. Fuel Process. Technol. 149, 29–39.
Torkaman, N.F., Bremser, W., Wilhelm, R., 2023. Catalytic recycling of thermoset carbon fiber-reinforced polymers. ACS Sustain. Chem. Eng. 12, 7668–7682.
Tortorici, D., Chen, Y., Mishnaevsky Jr, L., Laurenzi, S., 2025. Recycling carbon fibers by solvolysis: effects of porosity and process parameters. Compos. A: Appl. Sci. Manuf. 190, 108667.
Vrentas, J.S., Vrentas, C.M., 1998. Dissolution of rubbery and glassy polymers. J. Polym. Sci. B Polym. Phys. 36 (14), 2607–2614.
Wallmersperger, T., Ballhause, D., Kröplin, B., Günther, M., Gerlach, G., 2009. Coupled multi-field formulation in space and time for the simulation of intelligent hydrogels. J. Intell. Mater. Syst. Struct. 20 (12), 1483–1492.
Wiegand, S., 2004. Thermal diffusion in liquid mixtures and polymer solutions. J. Phys. Condens. Matter 16 (10), R357.
Xu, P., Li, J., Ding, J., 2013. Chemical recycling of carbon fibre/epoxy composites in a mixed solution of peroxide hydrogen and N, N-dimethylformamide. Compos. Sci. Technol. 82, 54–59.
Yan, H., Lu, C., Jing, D., Chang, C., Liu, N., Hou, X., 2016. Recycling of carbon fibers in epoxy resin composites using supercritical 1-propanol. N. Carbon Mater. 31 (1), 46–54.
Yu, K., Yang, H., Dao, B.H., Shi, Q., Yakacki, C.M., 2017. Dissolution of covalent adaptable network polymers in organic solvent. J. Mech. Phys. Solid. 109, 78–94.
Zeng, X., et al., 2017. Structure-induced variation of thermal conductivity in epoxy resin fibers. Nanoscale 9 (30), 10585–10589.
Zhang, J., Lin, G., Vaidya, U., Wang, H., 2023. Past, present and future prospective of global carbon fibre composite developments and applications. Compos. B Eng. 250, 110463.
Collaborative project for recycling wind turbine blades boosts circularity in fossil-free wind power; Stena Recycling, 2023-12-08. Link: https://www.stenarecycling.com/news-insights/newsroom/2023/wind-turbine-blade-recycling-boosts-circularity-in-fossil-free-wind-energy/,.